Turkish Journal of Electrical Engineering & Computer Sciences

http://journals.tubitak.gov.tr/elektrik/

Research Article

Turk J Elec Eng & Comp Sci
(2017) 25: 2660 – 2673

doi:10.3906/elk-1511-75

Intelligent reorganized discrete cosine transform for reduced reference image quality assessment

Tariq BASHIR[1,*], Imran USMAN[2], Shahnawaz KHAN[2], Junaid ur REHMAN[3]
[1]Department of Electrical Engineering, COMSATS Institute of Information Technology, Islamabad, Pakistan
[2]College of Computing and Informatics, Saudi Electronic University, Riyadh, Saudi Arabia
[3]Electronics and Radio Engineering Department, Communication and Coding Theory Lab (CCTLab), Kyung Hee University, Suwon, South Korea

Received: 08.11.2015 • **Accepted/Published Online:** 13.10.2016 • **Final Version:** 30.07.2017

Abstract: Reduced reference image quality assessment does not require the presence of the original image for assessing the quality of a degraded image. This work proposes an intelligent method for reduced reference image quality assessment based on a reorganized discrete cosine transform (RDCT). A genetic algorithm (GA) is used to compute optimized estimation of the generalized Gaussian distribution (GGD), which then approximates the coefficient distribution in the RDCT domain. Experimental results validate that such an intelligent estimation produces far superior results compared to conventional empirical estimation methods as presented in the literature. We compare the proposed technique with a number of contemporary techniques in the literature and demonstrate the generalization capability and effectiveness of the proposed technique as compared to prior works.

Key words: Reduced-reference image quality assessment (RR-IQA), reorganized discrete cousin transform (RDCT), generalized Gaussian distribution (GGD), genetic algorithm (GA)

1. Introduction

Modern day life very much depends on a broad range of digital applications ranging from high definition multimedia, smart phones, and tablets to internet gaming and video streaming. In addition to the multimedia world, the advent and widespread of faster and cheaper computing and communication devices has brought many advances in other fields as well, including medical imaging, aerial photography, remote sensing, and digital watermarking, to name a few. Due to this prevalence of technology, the ease of acquisition, storage, and transmission of digital images has increased significantly over the last decade. During all these operations, digital images are susceptible to various kinds of legitimate and illegitimate distortions. These distortions, or perceptual degradations, necessitate the image quality assessment evaluation process to be resource efficient and reliable. To evaluate the quality of degraded images, subjective and objective image quality assessment (IQA) [1–4] techniques are widely used in the literature.

Both subjective and objective IQA techniques have their own merits and demerits. As an example, in subjective quality assessment the final decision maker is the human eye or the physiological system pertaining to perception and its understanding, which may vary largely from person to person [2]. Since the end users are humans, in general it is a decent and reliable method for image quality assessment. Mean opinion score (MOS)

*Correspondence: tariq.haque81@gmail.com

[2–4] is one of the most widely used quality metrics for the assessment of subjective quality [3], whereby a number of human observers are considered to assess the quality of an image. Howbeit, it is time consuming and difficult for most applications. On the other hand, objective quality assessment methods do not require human involvement for the evaluation of IQA. Therefore, these techniques are more appropriate for most applications. Objective quality metrics can be grouped according to the presence of the original image or its absence at the time of quality evaluation of a potentially degraded image. In general, objective image quality assessment can be categorized into three groups [4]: full-reference image quality assessment (FR-IQA), no-reference image quality assessment (NR-IQA), and reduced-reference image quality assessment (RR-IQA).

FR-IQA [5] image quality assessment is a powerful technique for IQA and requires the presence of the original image at the time of quality evaluation. The most commonly used metrics for this type of IQA are peak signal to noise ratio (PSNR) and structural similarity index measure (SSIM). However, a full-reference image is not always present in most of the applications because of bandwidth and data storage limitations. Therefore, a method is desirable that evaluates image quality without any need for a full-reference image. The NR-IQA or blind IQA method needs no reference, or the original image, for evaluation of the distorted image. Quality estimation in the absence of a reference is very difficult. Therefore, most IQA techniques [6] strive to use priori knowledge of a set of specific distortion types to infer perceptual quality. In between FR-IQA and NR-IQA, there exists RR-IQA, in which some of the features are extracted and sent to the receiver through an ancillary channel for the evaluation of quality assessment. The RR-IQA method requires some of the image features as a reference for calculation of the distorted image. Figure 1 shows a generalized flow chart of RR-IQA. The transmitter sends only side information of the image through the ancillary channel as a reference for the receiver. This side information must be adequate enough such that the prediction errors are minimized.

2. Related work

Regarding FR-IQA, in [5] a psychometric study for subjective quality assessment is conducted for several prominent FR-IQAs and tested on different images for five distortion types. On the other hand, Wang et al. [6] proposed SSIM as an objective method for FR-IQA. SSIM [7–9] is based on the hypothesis that the human visual system (HVS) is highly adaptive in extracting structural information. It compares local patterns of pixel intensities that have been normalized for luminance and contrast. Lee et al. [8] modeled the nonuniform sampling that agrees with visual sensation at the human retina and calculates in curvilinear coordinates using the foveal signal to noise ratio (FSNR).

Gao et al. [10] proposed a new framework for RR-IQA based on city-block distance to measure the quantity of visually sensitive coefficients, Weber's law of just noticeable difference (JND), and contrast sensitivity function (CSF). Wang et al. [11] proposed the wavelet-domain natural image statistics model (WNISM), which measures image distortion by applying Kullback–Leibler divergence (KLD) between the marginal distributions of wavelet coef?cients of the reference and distorted images. However, the WNISM fails to consider statistical correlations of wavelet coefficients in different subbands and falls short in explicitly extracting geometrical information. In [11], the WNISM utilizes the generalized Gaussian distribution (GGD) for estimation of wavelet coefficients. KLD is applied to restore the perceptual quality of the distorted image. Tao et al. [12] utilized contrast sensitivity and JND in the contourlet domain to propose a novel RR-IQA technique.

Nevertheless, the WNISM has some limitations, which are investigated in detail by Ma et al. [13] and are summarized as: (a) the coefficient connectivity is not taken into account in the wavelet subbands [10]; (b) it performs well on a single distortion type but is not effective for multiple distortions when analyzed together [14];

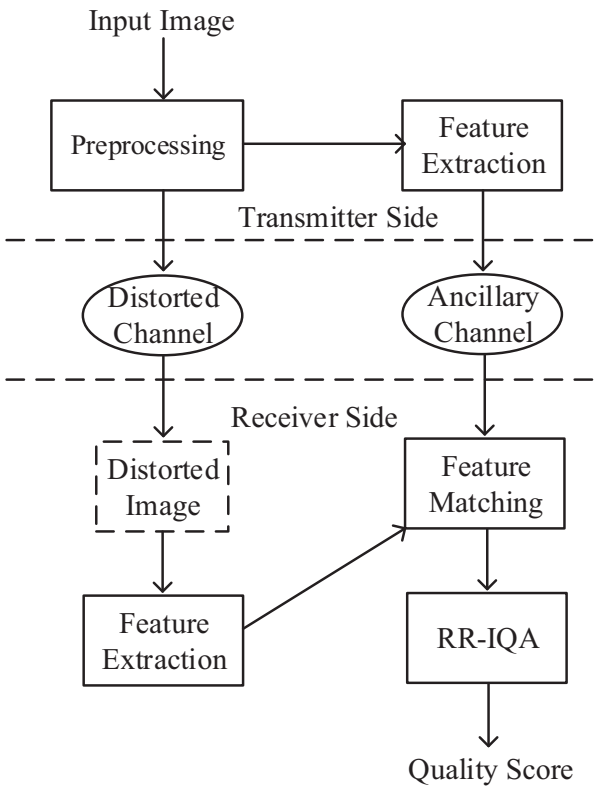

Figure 1. General architecture of RR-IQA system.

(c) in the case of KLD, it is computationally expensive when two different GGDs are computed [15], which indeed is not feasible for practical applications. In addition, since KLD is asymmetric [16], the distance between the distorted and original images is not the same. Ma et al. [13] empirically estimated the GGD of RDCT subbands that model the coefficient distribution of the subband. However, empirical estimation is not applicative in real world scenarios. We take up this deficiency as a basis of this work and propose an intelligent method that is viable to be implemented for practical applications and is generalized and image independent. To do so, the proposed technique utilizes a genetic algorithm (GA) and its inherent learning capabilities to optimize band specific GGD slopes. The quality metric performance of the proposed technique is tested through correlation coefficients (CC), Spearman rank order coefficient correlation (SROCC), and the traditional root mean square error (RMSE), which are elucidated in section 5. Experimental results substantiate the superiority of the proposed technique compared to existing techniques and its usefulness for practical applications.

The rest of the paper is organized as follows. Section 3 discusses details of the RDCT and GGD and describes some quality assessment methods. Section 4 explains our proposed intelligently structured image quality assessment technique (IS-IQA). Experimental results are presented and discussed in Section 5. Finally, section 6 concludes this work by presenting conclusion and some future directions.

3. Reorganized discrete cosine transform (RDCT)

The discrete cosine transform (DCT) belongs to the family of transforms that represents signals in terms of sinusoids of varying frequencies. When applied on 2D images, the transform is in the form of different oscillating

frequencies, i.e. horizontal and vertical. The RDCT, as the name suggests, fundamentally is based on the DCT. The only difference between an ordinary DCT and the RDCT is the process of reorganization. DCT is applied on blocks of 8 × 8 pixels followed by a reorganization process as depicted in Figure 2. Each location of these 8 × 8 blocks corresponds to a specific cosine having a horizontal and vertical frequency. Hence we can organize these values in order to get a better insight into its frequency content. In Figure 2a, firstly the 8 × 8 DCT coefficients are organized into three levels comprising ten subbands namely S0 to S9. S0, S1, S2, and S3 represent the first level; S4, S5, and S6 denote the second level, and the remaining subbands constitute the third level [17]. Then the corresponding coefficients from different DCT blocks are grouped together and organized according to their corresponding positions. For better visualization, DC components are scaled between 0 and 255 and their representation is in Figure 2b. The AC component is achieved by Eq. (3) and shown in Figure 2c. More details on such reorganization can be found in [13].

$$255 - (5 \times |AC|) \tag{1}$$

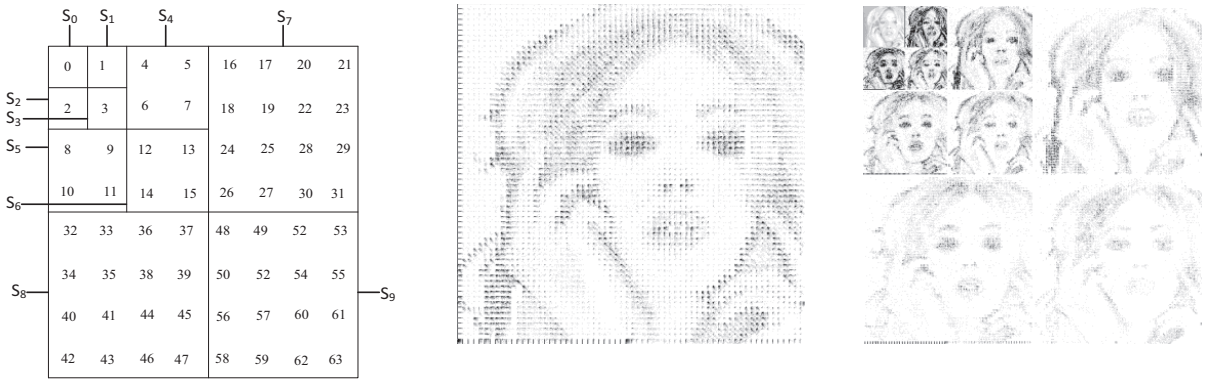

(a) 8×8 DCT Block can be treated as depth-3 tree of coefficient [17]

(b) 8×8 DCT Image Representation

(c) 8×8 RDCT Image Representation

Figure 2. Result of representation in RDCT.

3.1. DCT coefficients as GGD distribution

Based upon rigorous mathematical analysis, Lam et al. [18] showed that the high frequency DCT coefficients follow a kurtotic distribution that a GGD can easily conform to. That is, the normalized distributions of all AC bands follow the same trend as the GGD. The probability density function of a GGD is given by

$$p_{\alpha,\beta}(x) = \frac{\alpha}{2\beta\Gamma\left(\frac{1}{\alpha}\right)} \exp\left\{-\left(\frac{|x|}{\beta}\right)\right\}, \tag{2}$$

where $\alpha > 0$ and β are two parameters of the GGD function. They also govern the shape of the distribution. Γ is the Gamma function defined by

$$\Gamma(x) = \int_0^\infty t^{x-1} e^{-t} dt. \tag{3}$$

3.2. Reduced reference (RR) image quality assessment

It has been shown in the literature [13] that the coefficient histogram of the subbands of each reorganized DCT subband of the reference image can be best represented by a GGD model. Hence, for each GGD, two parameters, α and β, are required for RR-IQA. Since KLD is asymmetric, it is not a good method to calculate the visual quality of an image [16]. Based on this fact, we use city-block distance between the GGD of subbands of the original and the distorted images to estimate the difference in visual quality. The city block distance between two distributions h and g is given by

$$d_{city}(h,g) = \sum_{i=1}^{L} |h(i) - g(i)|, \tag{4}$$

where L represents the number of histogram bins. Therefore, the city-block distance between the actual distribution ρ and the GGD fitted distribution $\rho_{\alpha,\beta}$ of each reorganized DCT subband can be obtained by $d_{city}(\rho_{\alpha,\beta},\rho)$. It is to be noted that ρ is computed on the transmitter side and $\rho_{\alpha,\beta}$ is the GGD model approximation of the original image. Hence, for each reorganized DCT subband, three parameters $\{\alpha,\beta,d_{city}(\rho_{\alpha,\beta},\rho)\}$ are required to be transmitted to the receiver side for quality assessment. For details, we have adopted a procedure similar to that described in [13]. Once the image is received on the receiver side, the aim is to compute the city-block distance of the coefficient distributions of the original image and those of the distorted image ρ_d.

$$d_{city}(\rho,\rho_d) = \sum_{i=1}^{L} |\rho(i) - (\rho_d(i))|. \tag{5}$$

Since the coefficient distributions of the original image are not available on the receiver side, we estimate them by using the fitted GGD model. The prediction error approximates the city-block distance between the original and the distorted images. The inequality

$$\begin{aligned} &\sum_{i=1}^{L} |\rho_{\alpha,\beta}(i) - \rho_d(i)| - \sum_{i=1}^{L} |\rho(i) - \rho_{\alpha,\beta}(i)| \le \sum_{i=1}^{L} |\rho(i) - \rho_d(i)| \\ &\le \sum_{i=1}^{L} |\rho_{\alpha,\beta}(i) - \rho_d(i)| + \sum_{i=1}^{L} |\rho(i) - \rho_{\alpha,\beta}(i)| \end{aligned} \tag{6}$$

implies that $d_{city}(\rho,\rho_d)$ is bounded by

$$\begin{aligned} &d_{city}(\rho_{\alpha,\beta},\rho_d) - d_{city}(\rho_{\alpha,\beta},\rho) \le d_{city}(\rho,\rho_d) \\ &\le d_{city}(\rho_{\alpha,\beta},\rho_d) + d_{city}(\rho_{\alpha,\beta},\rho), \end{aligned} \quad . \tag{7}$$

We employ the lower bound to approximate the distance between the original and distorted images as done in [13] to give

$$d'_{city}(\rho,\rho_d) = d_{city}(\rho_{\alpha,\beta},\rho_d) - d_{city}(\rho_{\alpha,\beta},\rho). \tag{8}$$

In the case of a distorted image, we cannot fit ρ to a GGD model, as it is not suitable for depicting the distorted images. Hence, we compute the distance $\{\alpha,\beta,d_{city}(\rho_{\alpha,\beta},\rho)\}$ between the coefficient distribution of the distorted image and the fitted GGD of the reference image using Eq. (4). By considering the prediction error of the GGD modeling, we obtained the approximated distance using Eq. (8).

Finally, the visual distance between the original image and the distorted image is obtained by

$$\begin{aligned} V_{dist} &= \log_{10}\left(1+\tfrac{1}{c}\sum_{i=1}^{I}|d'^{i}_{city}(\rho^{i}.\rho^{i}_{d})|\right) \\ &= \log_{10}\left(c+\sum_{i=1}^{I}|d'_{city}(\rho^{i}.\rho^{i}_{d})|\right)-\log_{10}(c) \end{aligned}, \tag{9}$$

where i denotes the index of the reorganized DCT subband (ranging from 0 to 9) as shown in Figure 2, whereas c is used for scaling purpose in order to avoid V_{dist} being too small. For simplicity, the value for c is set to 0.0001.

4. Proposed intelligently structured image quality assessment technique (IS-IQA)

4.1. General architecture of the proposed technique

This section presents the details of our proposed IS-IQA technique. The proposed technique utilizes a GA and is composed of two phases, namely the training and the testing phase as shown in Figure 3. In the training phase, a number of images are used as a training data set in order to evolve suitable and generic values for α and β through extensive GA-based simulation. Once a suitable set of parameter values is obtained, it is then utilized in the testing phase in order to ascertain the generalization capability of the best evolved suitable parameter values, which govern the shape of the GGD slope. It is to be noted here that, although the training phase has a temporal cost, the best evolved parameter values are generalized and can be directly used in real world applications. Details of different modules are presented in the following subsections.

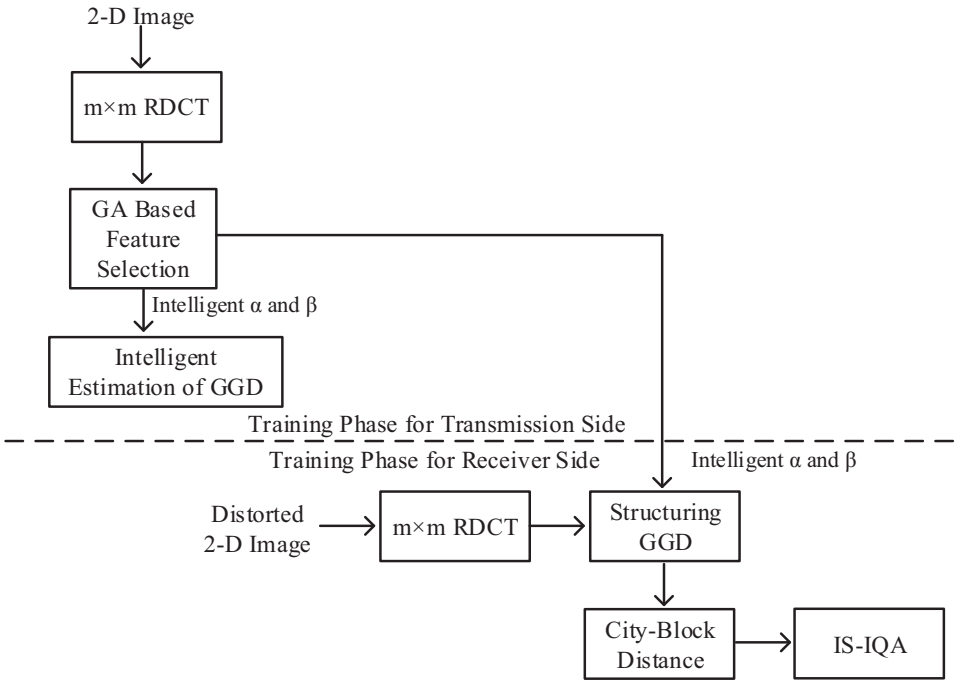

Figure 3. General architecture of the proposed IS-IQA technique.

4.2. GA-based training phase

The training phase is based on a number of training images that are utilized to compute the fitness value of each candidate solution in a GA population. A candidate solution comprises a pair of values encoded in the chromosome, or genome, of a GA. Initially, a random number of individuals, equal to the population size, are initialized with random values. Each individual chromosome is then scored by finding the visual distance between the original image and the distorted image using Eq. (9). Note that for doing so, the candidate values of the chromosome for α and β are used to estimate the slope of the GGD. These are also sent to the receiver side to approximate the visual quality of an image. In order to incorporate the performance of a candidate solution for a set of different images, we take the average of the visual distance values for the whole set. Let N be the total number of images in the training set. Then the fitness $Fitness_{i,G}$ of the ith candidate solution for the Generation G is given by

$$Fitness_{i,G} = \sum_{j=1}^{N} V_{dist(i,G)}, \tag{10}$$

It is to be noted that our objective is to minimize the fitness value as it is a minimization problem. Once all the individual candidate solutions in a population are scored, genetic operators of crossover, mutation, and replication are applied to create individuals for the next generation. These operators help to converge to the optimal solution and escape from trapping into local minima. The whole procedure continues generation by generation with scoring and creation of new generation in place until we reach a termination criterion. The termination criterion may be based upon an acceptable value of fitness, or a specific number of generations or time limit. In this work, we used the fitness value as the termination criterion for our GA simulations.

4.3. Testing phase

Once the training phase is complete, we save the best evolved parameter values for α and β. These values are then passed on to the testing phase to validate the usefulness of the best evolved solution for real world scenarios. Once the results on the testing data are up to an acceptable value, we keep those best evolved expressions as the final values for estimating the GGD slope. Otherwise, we run the simulation again and try to find another appropriate optimum solution.

5. Experimental results and discussion

This section explains the implementation details and presents the performance comparison of the proposed technique with the existing state of the art contemporary techniques.

5.1. Implementation details

The proposed technique is implemented in MATLAB 2013a using Intel Core i5 2.4 GHz. For the simulation of GA, the MATLAB R2013a based GA toolbox is utilized. The database used for training purpose and testing the accuracy of our proposed method consists of 29 images including standard images such as 'milk drop', 'tiffany', 'baboon', 'airplane', 'lake', 'peppers', and 'Lena'. In order to assess the performance of our generalized distribution and in the training phase, 13 images from LIVE Database from Middlebury and 9 standard images (22 images in total) are used. With the above setup, the proposed technique takes about 20 min for GA training simulation. Once the optimum parameter values are evolved, it takes a fraction of a second to do the image

quality assessment. In order to demonstrate different kind of distortions, we use JPEG 2000 compression, JPEG compression, additive white Gaussian noise (AWGN), Gaussian blur, and Rayleigh fast fading attack.

5.2. Performance comparison of the estimation error of the proposed IS-IQA technique

Figure 4 illustrates the pdf of the original frequency band coefficients compared with that computed using GGD for the technique presented in [13] and the proposed technique. Figure 4-IIa–f shows the pdf for different subbands from S4–S9 of the proposed method, whereas 4-Ia–f represents those computed using the Ma et al.'s method [13]. It can be seen from all the subbands that the GGD computed using the proposed IS-IQA generates less absolute estimation error, and hence the better capability to model the frequency distribution of the DCT coefficients. Subsequently, this will help in better image quality assessment on the receiver side. It is to be noted that for the middle frequency regions of an image, i.e. subbands S6–S8, there is a substantial improvement with the proposed technique as compared to the prior work. Thus, the proposed technique could also be very helpful for digital watermarking applications [19,20] that mostly utilize the middle frequency regions to conceal the watermark message bits.

Figure 5 demonstrates the performance of the proposed technique in terms of different images. The average error (comprising all the subbands) between the GGD computed by the proposed technique, steerable pyramid method [21], and Ma et al.'s method [13] is presented for a set of different images. It can be seen that for all the images, the proposed IS-IQA performs far better than the contemporary techniques. This improvement is due to the fact that the proposed technique is capable enough to exploit the hidden dependencies, and converging to the optimum value by stochastically exploring the solution space.

5.3. Performance comparison in terms of different objective measures

The performance of the proposed IS-IQA technique is also tested in the presence of different attacks that resemble the real world distortions an image is most likely subjected to. These include JPEG 2000, JPEG, AWGN, Gaussian blur, and fast fading attack. In order to quantify the performance comparison of different techniques, we use CC, SROCC, and MSE. For this, we adopt the performance evaluation procedure that is used in [13]. We let Q_i denote the visual quality index of the *ith* distorted image derived from the corresponding IQA method. The nonlinearity chosen for regression for each of the methods tested is a five-parameter $\{\Psi_1, \Psi_2, \Psi_3, \Psi_4, \Psi_5\}$, monotonic logistic function, such that Q_i is mapped to VQ_i.

$$VQ_i = \Psi_1 Logistic(\Psi_2, (Q_i - \Psi_3)) + \Psi_4 Q_i + \Psi_5, \tag{11}$$

$$Logistic(\tau, v) = \frac{1}{2} - \frac{1}{1 + \exp(\tau v)}. \tag{12}$$

After the nonlinear mapping procedure, the correlation coefficient (CC) is used to provide an evaluation of the prediction accuracy between the subjective scores and the nonlinear mapped objective scores. Larger CC values mean that the subjective and the objective scores have high correlation, thus leading to better performance of the IQA. The following subsections highlight the performance in terms of these measures.

5.4. Performance comparison of CC

CC can be expressed as values in the range of +1 and –1. A coefficient with a value of +1 indicates a perfect positive correlation. That is, the change in both the variables is in the same direction. A value of –1 specifies

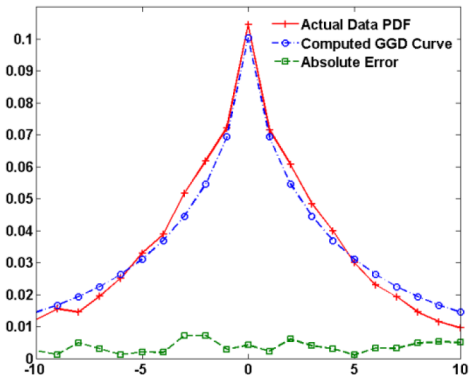

I(a) Distribution of S4

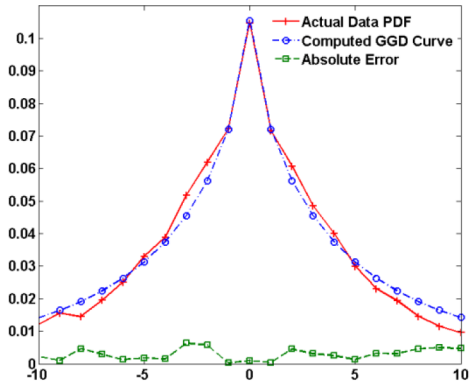

II(a) Distribution of S4

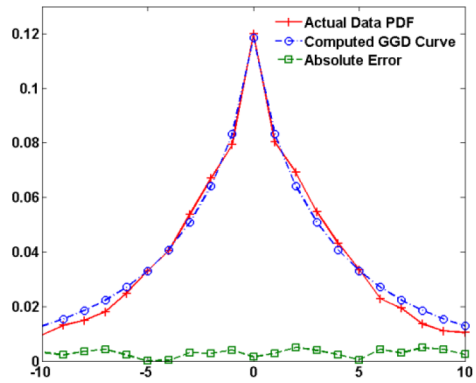

I(b) Distribution of S5

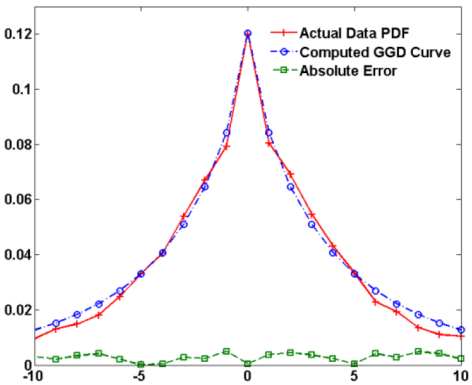

II(b) Distribution of S5

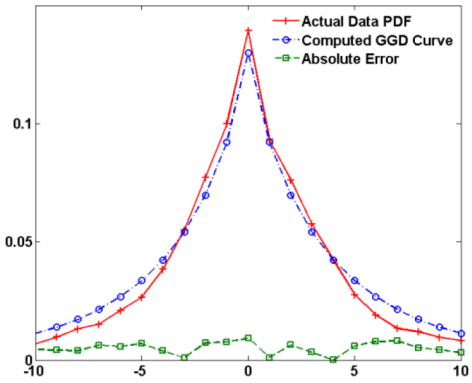

I(c) Distribution of S6

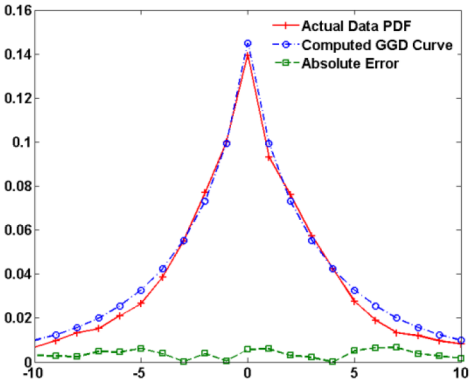

II(c) Distribution of S6

Figure 4. a)f). Actual distribution versus GGD computed distribution along with their absolute error for 6 subbands (I) with GGD set empirically, (II) GGD computed by the proposed IS-IQA technique. Note that prediction error is along the y-axis, whereas variance is shown along the x-axis.

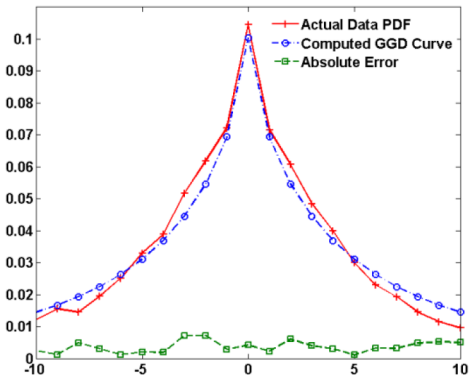

I(a) Distribution of S4

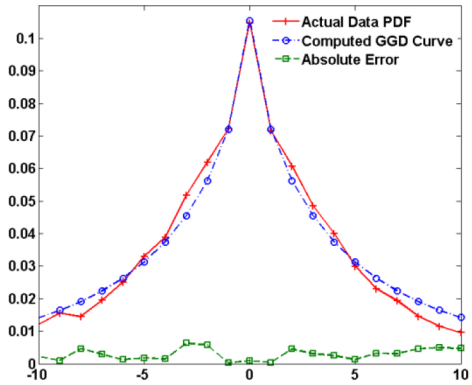

II(a) Distribution of S4

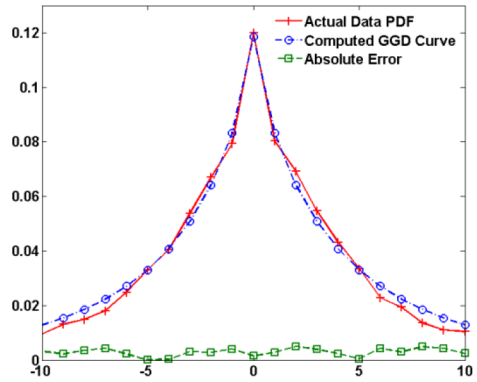

I(b) Distribution of S5

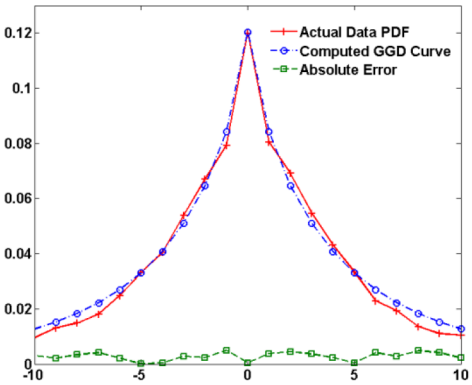

II(b) Distribution of S5

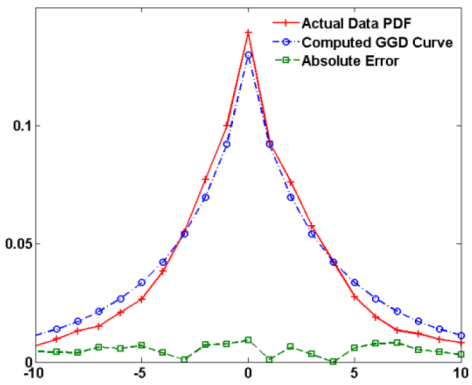

I(c) Distribution of S6

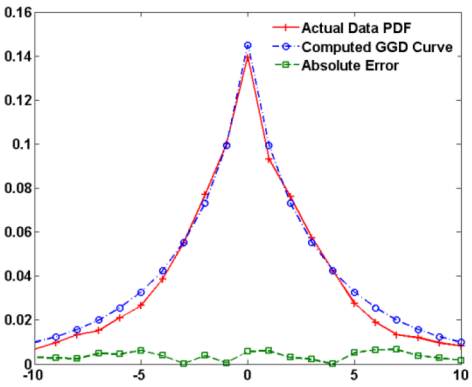

II(c) Distribution of S6

Figure 4. Continued.

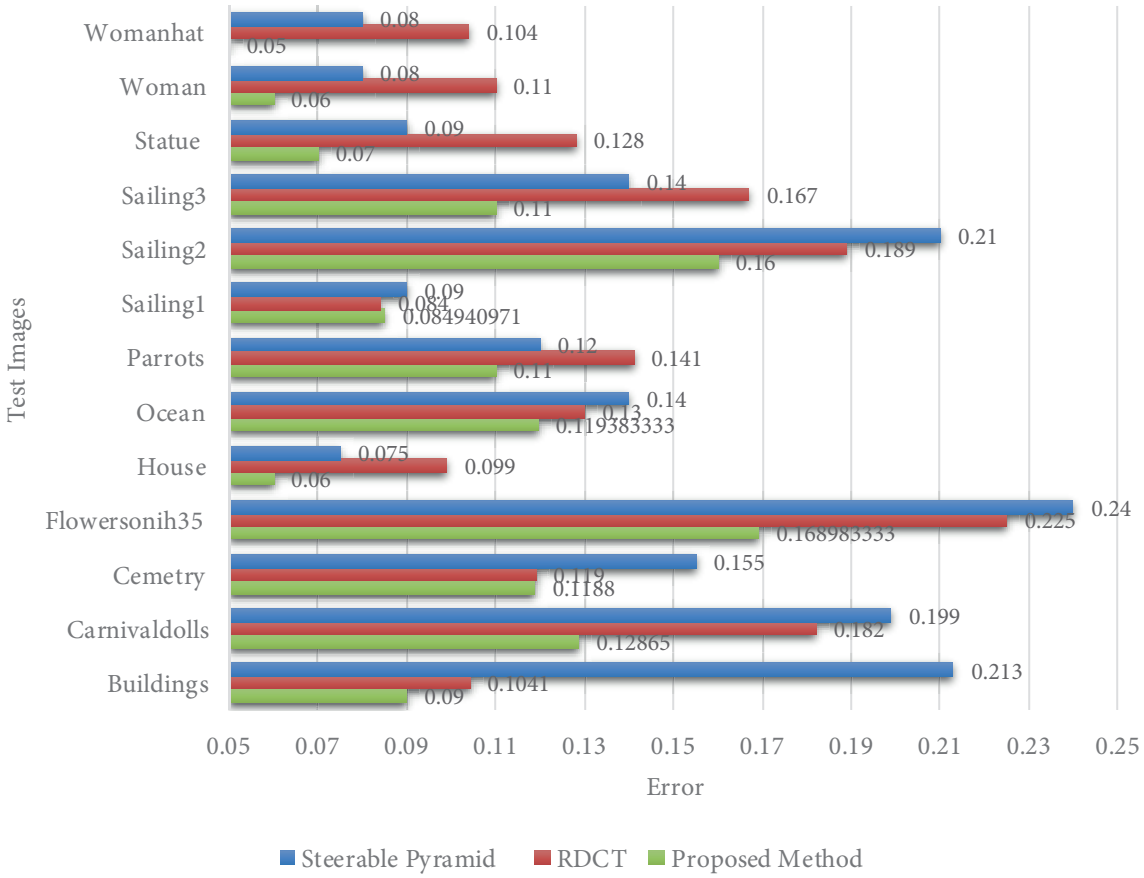

Figure 5. Comparison of estimation error between steerable pyramid, Mas RDCT, and the proposed technique.

a negative correlation, whereby the change in one variable is in the opposite direction of the other variable. Figure 6 displays the performance comparison of the proposed IS-IQA with a number of other IQA techniques including PSNR, WNISM, and Ma et al's RDCT based technique [13]. It can be observed that the proposed method outperforms all the contemporary techniques in most cases except for AWGN distortion. In this case, PSNR gives a better estimation of image quality.

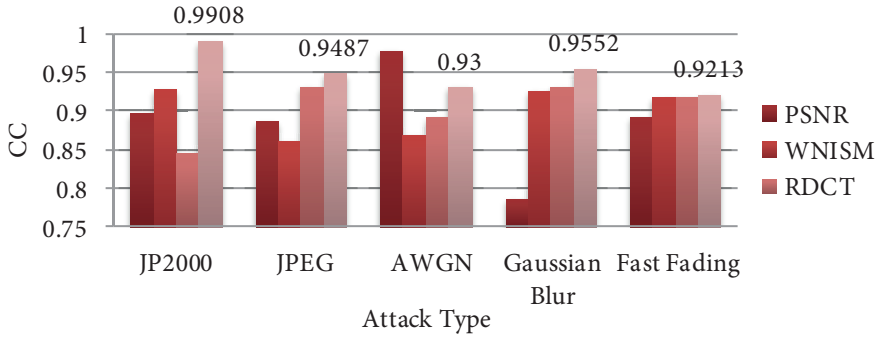

Figure 6. Performance comparison in terms of CC for different quality metrics with the proposed technique in the presence of different attacks.

5.5. Performance comparison of SROCC

The performance comparison in terms of SROCC is shown in Figure 7 for the proposed technique and other contemporary techniques. Again the proposed technique outperforms other existing techniques except for AWGN, where the PSNR gives better indication of the quality of an image. The reason for such an improvement is the intrinsic design of the PSNR metric, which is suitable for AWGN distortions. Apart from the PSNR IQA metric, the proposed technique performs better than the WNISM and Ma's RDCT techniques for AWGN as well.

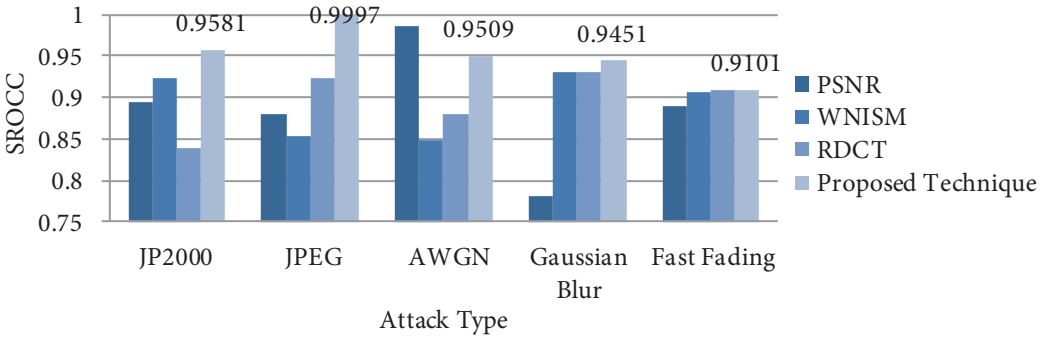

Figure 7. Performance comparison in terms of SROCC for different quality metrics with the proposed technique in the presence of different attacks.

5.6. Performance comparison of RMSE

The Table presents the performance in terms of RMSE for the proposed technique and contemporary techniques. The distortions taken into account include JPEG, JPEG 2000, AWGN, Gaussian blur, and fast fading channel distortion. It is to be noted that the lower the RMSE value, the better is the performance of a technique. From the Table, it can be seen that in terms of RMSE score as well, the proposed technique outperforms all the existing methods in the literature. Although there is a slight advantage to PSNR with respect to the IS-IQA for AWGN noise attack, as a whole, the proposed technique is far superior to the existing techniques in terms of RMSE.

Table. Performance comparison in terms of RMSE for different quality metrics with the proposed IS-IQA technique in the presence of different attacks.

Quality matrices	JP2K	JPEG	AWGN	Gaussian blur	Fast fading
PSNR	11.22	17.72	8.74	11.45	12.94
WNISM	9.37	16.17	13.87	6.96	11.31
RDCT	13.5	11.66	12.68	6.79	11.24
Proposed technique	9.1337	10.9542	11.349	5.9404	7.1981

5.7. Performance comparison in terms of generalization capabilities

Figure 8 demonstrates the generalization capability of the proposed technique using a box and whisker plot. A number of test images are used and the average absolute error is computed between the actual distribution and GGD based distribution for every image. The spread of the data for both the proposed technique (which uses intelligent parameter estimation for GGD) and the technique presented in [13] (which uses empirical parameter estimation) is demonstrated in the form of a box and whisker diagram. It can be observed that the minimum

and maximum error value for the whole sample data is much lower for the proposed technique as compared to [13]. Similar is the case for the first quartile, median, interquartile range, and third quartile. These results on the testing data verify the usefulness of the proposed technique for real world applications.

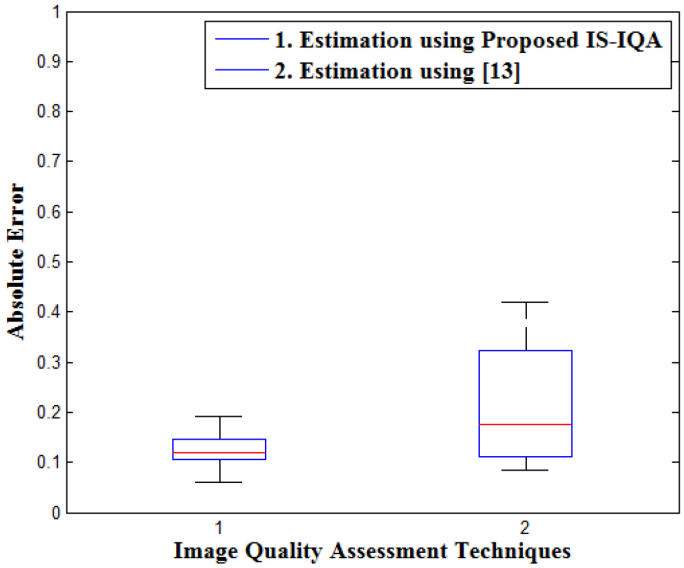

Figure 8. Comparison of empirical and intelligent GGDE.

5.8. Limitations of the proposed work

The temporal cost is the main drawback in the training phase of the proposed system because the GA uses a stochastic search and optimization of parameters. As discussed in the training phase, Eq. (9) is used to find the fitness value. Therefore, exhaustive GA simulation is required for the first time. Once the optimized parameters are calculated, only a fraction of time is required to embed a watermark in the cover image, which is more plausible for the real world scenario.

6. Conclusion

This paper presents a new method for RR-IQA based upon intelligent estimation of parameters for the GGD using a GA. We know that RDCT based coefficient distribution can be approximated with the GGD. However, empirical approximation techniques do not exploit the solution space properly, and hence lack in finding the optimum solution. We take advantage of the learning capabilities of the GA and its stochastic search in less temporal cost as compared to other intelligent techniques. When tested on real world data, we find that the proposed technique is generalized enough and outperforms the previous IQA techniques in the literature. One drawback of the proposed technique is the time it takes for a GA simulation to complete. However, in some applications, the improvement in yielding better RR-IQA is more desirable as compared to the temporal cost. In future, we will try to exploit further hidden dependencies using genetic programming.

Acknowledgements

The authors highly acknowledge the support provided by COMSATS Institute of Information Technology, Islamabad, Pakistan, for its in-house PhD program and the research facilities and support provided by Saudi Electronic University, Saudi Arabia.

References

[1] Zhou W, Bovik AC, Ligang L. Why is image quality assessment so difficult? In: IEEE International Conference on Acoustics, Speech and Signal Processing; 13–17 May 2002; Orlando, FL, USA: IEEE. pp. 4:3313-3316.

[2] Sheikh HR, Bovik AC. Image information and visual quality. IEEE T Image Process 2006; 15: 430-444.

[3] Wang Z, Sheikh HR, Bovik AC. Objective video quality assessment. In: Furht B, Marqure O, editors. The Handbook of Video Databases: Design and Applications. New York, NY, USA: CRC Press, 2003. pp. 1041-1078.

[4] Kim HT, Raveendran P. A survey of image quality measures. In: International Conference for Technical Postgraduates; 14–15 Dec. 2009; Kuala Lumpur, Malaysia: IEEE. pp. 1-4.

[5] Sheikh HR, Sabir MF, Bovik AC. A Statistical Evaluation of Recent Full Reference Image Quality Assessment Algorithms. IEEE T Image Process 2006; 15: 3440-3451.

[6] Wang Z, Bovik AC, Simoncelli E. Structural Approaches to Image Quality Assessment. In: Bovik AC, editor. Handbook of Image and Video Processing. New York, NY, USA: Academic Press, 2005. pp. 961-974.

[7] Zhou W, Bovik AC, Sheikh HR, Simoncelli EP. Image quality assessment: from error visibility to structural similarity. IEEE T Image Process 2004; 13: 600-612.

[8] Sanghoon L, Pattichis MS, Bovik AC. Foveated video quality assessment. IEEE T Multimedia 2002; 4: 129-132.

[9] Sheikh HR, Bovik AC, Cormack L. No-reference quality assessment using natural scene statistics: JPEG2000. IEEE T Image Process 2005; 14: 1918-1927.

[10] Gao X, Lu W, Tao D, Li X. Image quality assessment based on multiscale geometric analysis. IEEE T Image Process 2009; 18: 1409-1423.

[11] Wang Z, Simoncelli EP. Reduced-reference image quality assessment using a wavelet domain natural image statistics models. In: International Society for Optics and Photonics; 18 March 2005; San Jose, CA, USA. IS&T/SPIE. pp. 149-159.

[12] Tao D, Li X, Lu W, Gao X. Reduced-reference IQA in contourlet domain. IEEE T Syst Man Cy B 2009; 39: 1623-1627.

[13] Lin M, Songnan L, Fan Z, King NN. Reduced-reference image quality assessment using reorganized DCT-based image representation. IEEE T Multimedia 2011; 13: 824-829.

[14] Qiang L, Zhou W. Reduced-reference image quality assessment using divisive normalization-based image representation. IEEE J Sel Top Signa 2009; 3: 202-211.

[15] Li L, Tong CS, Choy SK. Texture classification using refined histogram. IEEE T Image Process 2010; 19: 1371-1378.

[16] Cover TM, Thomson JA. Elements of Information Theory. 2nd ed. Hoboken, NJ, USA: Wiley, 2006.

[17] Xiong Z, Guleryuz OG, Orchard MT. A DCT-based embedded image coder. IEEE Signal Proc Let 1996; 3: 289-290.

[18] Lam EY, Goodman JW. A mathematical analysis of the DCT coef?cient distributions for images. IEEE T Image Process 2000; 9: 1661-1666.

[19] Naheed T, Usman I, Khan TM, Dar AH, Shafique MF. Intelligent reversible watermarking technique in medical images using GA & PSO. International Journal for Light and Electron Optics 2011; 125: 2515-2525.

[20] Usman I, Khan A, Chamlawi R. Employing intelligence in the embedding and decoding stages of a robust watermarking system. AEU-International Journal of Electronics and Communications 2011; 65: 582-588.

[21] Simoncelli EP, Freeman WT, Adelson E H, Heeger DJ. Shiftable multi-scale transforms. IEEE T Inform Theory 1992; 38: 587-607.